SCIENTIFIC REPORTS

OPEN

SUBJECT AREAS:
ELECTRONIC PROPERTIES AND DEVICES
RAMAN SPECTROSCOPY
CHARACTERIZATION AND ANALYTICAL TECHNIQUES
OPTICAL PROPERTIES AND DEVICES

Received
16 April 2013

Accepted
17 July 2013

Published
5 August 2013

Correspondence and requests for materials should be addressed to A.T. (Antoine.Tiberj@univ-montp2.fr)

Reversible optical doping of graphene

A. Tiberj[1,2], M. Rubio-Roy[3], M. Paillet[1,2], J. -R. Huntzinger[1,2], P. Landois[1,2], M. Mikolasek[1,2], S. Contreras[1,2], J. -L. Sauvajol[1,2], E. Dujardin[3] & A. -A. Zahab[1,2]

[1]Université Montpellier 2, Laboratoire Charles Coulomb UMR 5221, F-34095, Montpellier, France, [2]CNRS, Laboratoire Charles Coulomb UMR 5221, F-34095, Montpellier, France and, [3]CEMES-CNRS, Université de Toulouse, 29 rue Jeanne Marvig, Toulouse 31055, France.

The ultimate surface exposure provided by graphene monolayer makes it the ideal sensor platform but also exposes its intrinsic properties to any environmental perturbations. In this work, we demonstrate that the charge carrier density of graphene exfoliated on a SiO_2/Si substrate can be finely and reversibly tuned between hole and electron doping with visible photons. This photo-induced doping happens under moderate laser power conditions but is significantly affected by the substrate cleaning method. In particular, it requires hydrophilic substrates and vanishes for suspended graphene. These findings suggest that optically gated graphene devices operating with a sub-second time scale can be envisioned and that Raman spectroscopy is not always as non-invasive as generally assumed.

Optical and electronic properties of graphene can be modulated by continuously tuning the charge carrier density using electrostatic gating[1–6], electrochemical doping[7] or charge transfer by adsorption of molecular species[8–23]. Besides electronic transport, the doping of graphene has a marked effect on the fundamental electron-phonon interactions, like the breakdown of the adiabatic Born-Oppenheimer approximation[1–4], the interplay between adiabatic and non-adiabatic effects[23] or the interference between all the quantum pathways involved in inelastic light scattering[5]. These effects have been conveniently investigated by Raman spectroscopy, which is also sensitive to the number of layers[24], their stacking ordering[25–28], the nature and density of defects[29–31] and the in-plane strain variations[32,33]. As a consequence, Raman spectroscopy of active modes in graphene, like the G and 2D bands, is being considered as a high-throughput technique to characterize graphene and to probe the inelastic light scattering phenomena. Moreover, several groups[24,34,35] have reported that no significant spectral changes were observed by collecting Raman spectra of graphene exfoliated on SiO_2/Si substrate, with a laser power P_{laser} ranging from 0.04 to 4 mW. Therefore, Raman spectroscopy is considered as non-invasive when performed with P_{laser} in the mW range.

Yet, the non-invasive character of Raman spectroscopy has been questioned by the reports of possible photo-induced effects and some authors recommended to use more cautious experimental conditions (laser power limited to 70 μW[36] or Ar annealing[34]). Laser irradiation has even been shown to induce irreversible damages of graphene[37,38]. Here, we report that the charge carrier density of exfoliated graphene lying on a hydrophilic SiO_2/Si substrate can be finely and reversibly tuned optically with visible photons. The influence of the laser power and the surface chemistry of the SiO_2/Si substrate on the optical doping of exfoliated graphene in air is examined. Our results also imply that Raman spectroscopy of graphene performed with usual experimental conditions (1 mW under a 100× objective) can be invasive as it directly alters the charge carrier density.

Results

In a first series of experiments, Raman spectra of exfoliated graphene excited with a 532 nm laser are collected as a function of the incident laser power, P_{laser}, at a fixed location. The results obtained for three different types of samples are compared. F1 was exfoliated on a hydrophilic SiO_2/Si substrate, F2 on a less hydrophilic substrate and F3 was suspended over a trench etched into the substrate (see methods). The quality of the samples is preserved during the whole experiments, as evidenced by the absence of the D band (see Supplementary Fig. S1c). All Raman spectra are fitted by Lorentzian functions to extract the position of the G band (ω_G), the full width at half maximum (FWHM) of the G band (Γ_G), the 2D band position (ω_{2D}) and the ratio between the integrated intensities of the 2D and G bands (A_{2D}/A_G).

For the sample F1, P_{laser} is increased from 0.05 mW up to 1.5 mW and decreased back to 0.05 mW, as shown in Figure 1. The G band at 1580 cm^{-1} for P_{laser} = 0.05 mW downshifts to reach a minimum value 1576.5 cm^{-1} for P_{laser} = 0.5–0.6 mW. With the further increase of P_{laser}, it upshifts up to 1579 cm^{-1} (Fig. 1a). Correspondingly, Γ_G rises from 7 cm^{-1} up to 12 cm^{-1} for P_{laser} = 0.5–0.6 mW and then decreases to 10 cm^{-1} (Fig. 1b). In the same

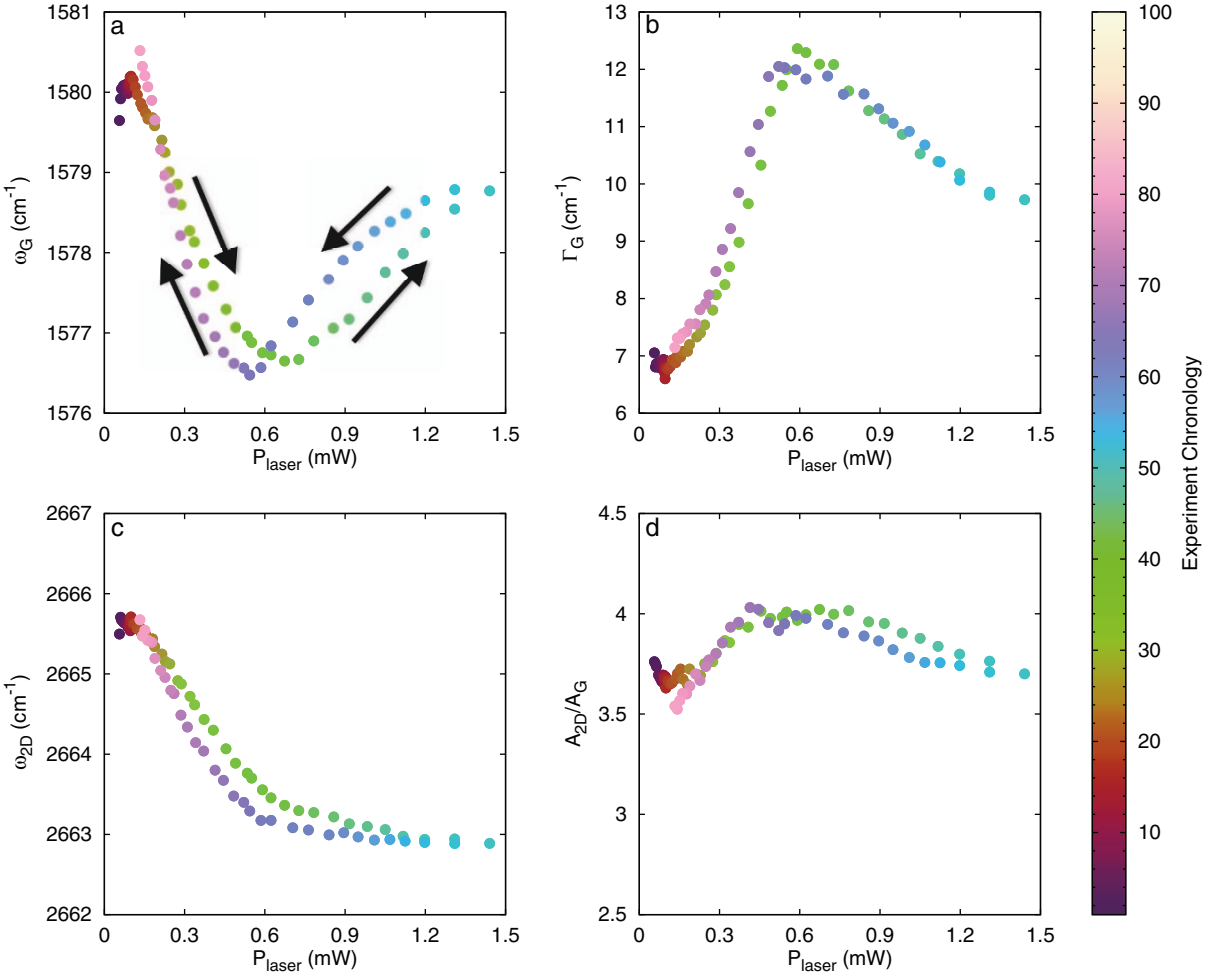

Figure 1 | Reversible evolution of Raman spectra as a function of the incident laser power P_{laser} for the graphene flake F1. (a) the G band position ω_G, (b) the G band FWHM Γ_G, (c) the 2D band position ω_{2D} and (d) the integrated intensities ratio A_{2D}/A_G. The graphene flake F1 is exfoliated on a hydrophilic substrate. P_{laser} is increased from 0.05 mW up to 1.5 mW and decreased back to 0.05 mW as shown by the arrows in (a). The color code of each point corresponds to the chronological order in which the measurements have been carried out as depicted on the right hand side color bar (for the corresponding time see Supplementary Fig. S2).

conditions, the 2D band continuously downshifts from 2666 cm^{-1} down to 2663 cm^{-1} (Fig. 1c). The A_{2D}/A_G ratio displays a maximum for P_{laser} around 0.5–0.6 mW (Fig. 1d). The comparison of the concomitant evolution of ω_G, ω_{2D}, Γ_G and A_{2D}/A_G with electrostatic gating results[1–4] indicates that the graphene doping is modified upon light irradiation. In particular, the coincidence of the maxima of Γ_G and of A_{2D}/A_G with the minimum of ω_G is a signature of neutral graphene. The doping type is determined from the evolution of ω_{2D}[3,4]: a larger upshift for p-doping (below 0.5–0.6 mW) than for low-level n-doping (above 0.5–0.6 mW). Interestingly, the changes are observed to be mostly reversible when P_{laser} is decreased back to its initial value (Fig. 1). The doping of graphene deposited on a hydrophilic SiO_2/Si substrate can be continuously and reversibly tuned from the initial p-doping to quasi-neutral and eventually n-doping with moderate laser power. From the shifts and widths of the G band[3,4], the inital doping of F1 was estimated to be $p \approx 4 \times 10^{12}$ cm^{-2} at 0.05 mW. For $P_{laser} = 1.44$ mW, the carrier density was estimated to be $n \approx 3 \times 10^{12}$ cm^{-2}. Similar observations were made with different laser wavelengths: 488 nm, 514 nm and 660 nm (see Supplementary Figs. S3, S4, S5, and S6).

We now examine the influence of the underlying substrate by comparing these results to the ones obtained on sample F2 deposited on a less hydrophilic substrate and to sample F3 suspended over a trench etched into the substrate. The relative variations of the 2D and G band positions as a function of P_{laser} are collected in Figure 2. This particular representation disentangles doping and strain effects[33]. We clearly observe three different behaviors in the plots presented on Figure 2. When the doping of graphene is continuously tuned from p-type to n-type, the 2D versus G positions presents the particular v-shape shown in Figure 2a. The G band consistently upshifts with an increasing charge carrier density (for both electrons and holes). The 2D band downshifts monotonically as the doping varies from p to n. Figure 2b displays the 2D vs G behavior for a flake lying on a less hydrophilic substrate. The G and 2D bands continuously upshift as P_{laser} increases. The small upshift of the 2D band is expected for low level n-type doping[3,4,23]. Here, Γ_G is maximum for the lowest incident power and continuously decreases with the increasing laser power, and so does the A_{2D}/A_G ratio (see Supplementary Fig. S7 and S9). Considered together, these variations indicate that this supported graphene is close to neutral for the lowest P_{laser} and becomes n-doped as P_{laser} is increased (for $P_{laser} = 2.6$ mW, $n \approx 4$–5×10^{12} cm^{-2} from refs. 3 and 4). Once again, these doping variations are reversible when P_{laser} is decreased back. For the suspended graphene flake, F3, the high values of Γ_G (14 cm^{-1}) and A_{2D}/A_G ratio (9.5) remain constant through the entire power sweep (Supplementary Fig. S8). This indicates that F3 remains neutral as the laser power increases in agreement with S. Berciaud *et al.*[35] Thus, the small shifts of ω_G and ω_{2D} (Fig. 2c) cannot be ascribed to any doping level variation.

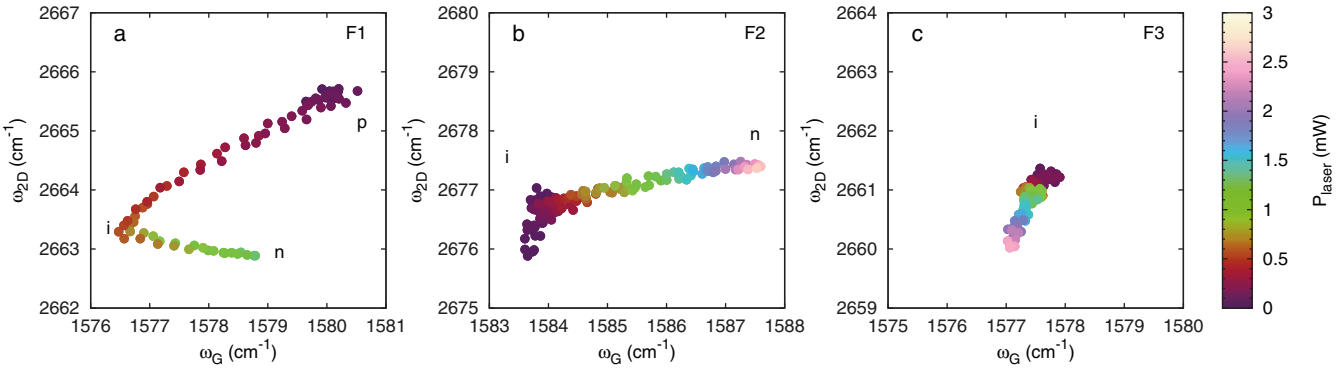

Figure 2 | Comparison of the relative evolutions of the 2D band position (ω_{2D}) versus the G band position (ω_G) as a function of P_{laser} for three graphene flakes (F1, F2 and F3). F2 was exfoliated on a less hydrophilic SiO_2/Si substrate than F1. F3 was suspended over a trench etched into the substrate. The color code of each point corresponds to the incident laser power P_{laser} as displayed on the right hand side color bar. (a) F1 is p-doped at low P_{laser}, it becomes quasi-neutral around 0.5 mW and n-doped for higher P_{laser}. (b) F2 is initially quasi-neutral and becomes n-doped with the increasing P_{laser}. (c) The suspended graphene flake, F3, is neutral and stays neutral with the increasing P_{laser}. The measured shifts for F3 are only due to laser heating effects. The different G band and 2D band positions (ω_G, ω_{2D}) of the different graphene samples (F1, F2, F3) in their quasi-neutral state are attributed to strain fluctuations from one sample to the other.

We can now wonder whether these laser-induced doping variations are uniform across the graphene surface. To this end, Raman mapping was performed at different laser powers on graphene exfoliated onto a hydrophilic substrate and partially suspended over a pre-patterned trench (sample F4, see optical microscopy image in supplementary Fig. S1b where the mapped area is shown). Maps of the ω_G, Γ_G, ω_{2D} and A_{2D}/A_G are displayed on Figure 3 for seven P_{laser} ranging from 0.1 mW to 3 mW. The constant position of the G and 2D bands across the whole supported area of the sample indicates that the strain and doping are homogeneous, therefore allowing to single out the influence of optical doping by the varying laser power. When the laser power is increased from 0.1 mW to 1.5 mW, the G band, initially at 1584 cm^{-1} (Γ_G = 7.5 cm^{-1}) shifts down to 1582 cm^{-1} (Γ_G = 12 cm^{-1}). Further increase of the laser power inverts the effect and the G band upshifts back to 1583.5 cm^{-1} (Γ_G decreases down to 9.5 cm^{-1}). For the same power sweep, the 2D band continuously downshifts from 2676 to 2672 cm^{-1}. Similarly, the A_{2D}/A_G ratio increases from 4.7 for P_{laser} = 0.1 mW, to 5.1 for P_{laser} between 0.5 and 1.5 mW, and then decreases back to 4.7 for higher laser powers. These observations confirm that graphene supported on hydrophilic SiO_2 evolves continuously from p-type to n-type doped graphene when the laser power is increased.

Interestingly, the irradiation of the suspended graphene yields a very different behavior. Indeed, Figure 3 shows that both G and 2D bands downshift from 1581.5 to 1578.5 cm^{-1} and from 2673 to 2663.5 cm^{-1} respectively as the laser power is increased. However, Γ_G and the A_{2D}/A_G ratio remain constant (13 cm^{-1} and 5.9 respectively). Therefore the doping level remains unchanged through the entire power sweep and the downshifts of the 2D and G bands are ascribed to classical laser-induced heating effects that are also observed on sample F3 (see Supplementary Fig. S8, S11 and S12).

A careful examination of the signals recorded on the graphene edges and on the trench contour reveals that the optical doping is less effective in these specific locations. In particular, the doping

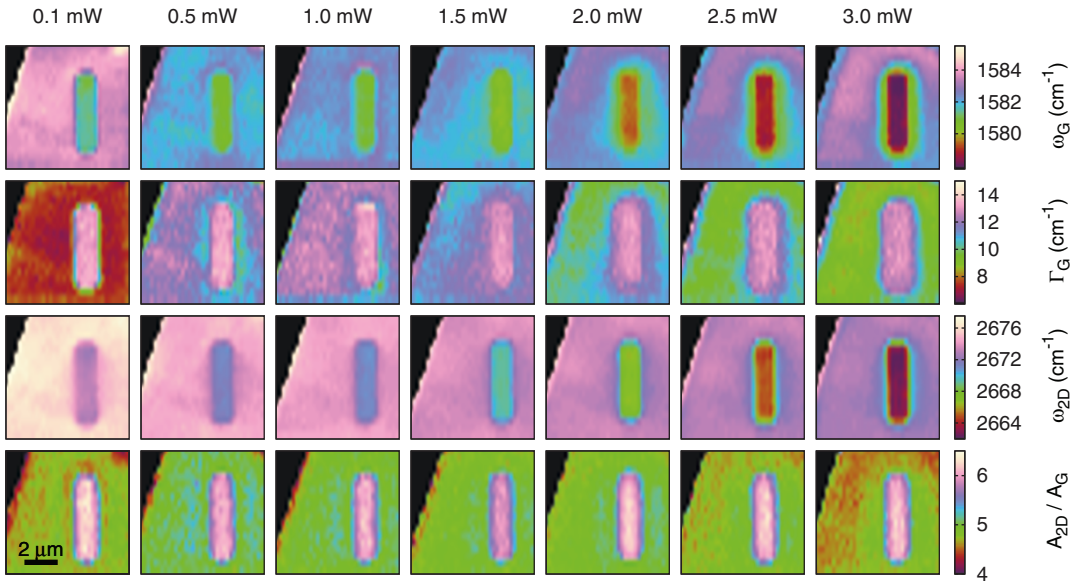

Figure 3 | Raman maps measured for 7 different laser powers on sample F4. The rows correspond from top to bottom to the G band position ω_G, the G band FWHM Γ_G, the 2D band position ω_{2D}, and the integrated intensities ratio A_{2D}/A_G. The graphene flake is covering an etched pool of the substrate that has a capsule shape and is visible on the right hand side of each map. The black upper left corners correspond to bare SiO_2/Si surfaces. A greyscale version of this figure is available as Supplementary Fig. S10.

never reaches n-type even for the highest P_{laser}. We attribute this local effect to the supplementary p-doping near graphene edges which has already been observed by Raman spectroscopy[39,40].

Discussion

The absence of doping upon irradiation of suspended graphene clearly shows that the substrate contributes to the mechanism involved in the optical doping of graphene. We thus investigated the influence of substrate cleaning procedures on the efficiency of the optical doping. For highly hydroxylated (hydrophilic) substrates, freshly cleaned by O_2 plasma and/or piranha treatments prior to graphene deposition, we observe the ambipolar behavior with a doping evolving from p-type to n-type upon increasing laser power. Our results confirm that graphene exfoliated on a hydrophilic substrate is p-doped[41,42] in contrast to the quasi-intrinsic state of suspended graphene[35]. Across the different samples studied here, we found that the P_{laser} for which graphene is neutralized falls in the range 0.5–2 mW. These values depend on the laser power density (laser spot size, see Supplementary Fig. S14) and graphene absorption (laser wavelength and SiO_2 thickness, see Supplementary Figs. S3, S4, S5, and S6). The density of hydroxyl groups can be reduced by performing a thermal annealing of the samples under argon before graphene deposition. In this case, graphene was observed to be initially quasi-neutral and n-type doping was obtained upon illuminating the sample with increasing P_{laser}. Finally, when graphene is transferred onto substrates used as-received without any cleaning, the doping of some flakes remain constant for all the entire P_{laser} range (not shown). Therefore, the absence of any significant spectral changes previously observed[24] might be accounted for by the deposition of graphene on as-received substrates. Finally, it should be pointed out that the optical doping is not specific to graphene micromechanically exfoliated onto SiO_2/Si substrates but similarly occurs for graphene deposited on standard glass (not shown).

It thus appears that the starting value of the graphene doping level is directly linked to the substrate preparation. Cleaning procedures that render the substrate hydrophilic tend to result in more p-doped supported graphene, in agreement with previous studies[43–47], which also demonstrated the involvement of adsorbed water in the p-doping of graphene by atmospheric oxygen[36,42,45,47,48]. Irreversible or slow modulation of charge carrier density was demonstrated by changing the atmosphere[36,42] or by illuminating graphene with UV or visible light[36,37,49]. In the latter cases, the invoked mechanisms relied on dopant removal and more specifically oxygen derivatives. The characteristic times of such phenomena were found to be in the range of minutes[36,49] or even hours[37]. Other authors have probed the dynamics of charge transfer between the H_2O/O_2 redox couple and graphene by electrical measurements alone or combined with Raman spectroscopy. It was shown that the equilibrium is established after minutes[48] or hours[42].

Our study shows that the charge carrier density can be conveniently tuned by adjusting the incident laser power even without a gating electrode. This effect does not involve the chemical modification of graphene since no D band emerges upon extended irradiation. By contrast with previous reports[36,37,49], this laser-induced doping is reversible with a characteristic time that was preliminarily evaluated to be less than 1 s (see Supplementary Fig. S15), *i.e.* orders of magnitude faster. This suggests that this phenomenon, although related to similar environmental effects, involves a different mechanism. O_2 and H_2O are playing a key role as illustrated by the weak dependency of ω_G on P_{laser} found after adsorbates removal by Ar annealing at 150°C of graphene lying on O_2 plasma treated SiO_2/Si substrates[34]. The transfer of "hot" electrons from optically excited graphene to the H_2O/O_2 redox couple or O_2^- superoxide anion proposed in reference 36 could only increase the hole doping in graphene upon visible light exposure, which is not supported by our observations. To get more insight on the underlying mechanism of the observed effect, we have measured the evolution of the G-band Stokes/AntiStokes integrated intensity ratio as a function of P_{laser} (see Supplementary Fig. S11). We were thus able to establish that, for graphene lying on a substrate, its local temperature increases by about 100°C/mW. This behavior was found to be similar for all the substrates tested (hydrophilic or less hydrophilic, 285 nm or 90 nm of SiO_2). Considering the occurence of a possible thermoelectric effect, the thermoelectric voltage that can build up in our experiments is expected to be of the order of few mV/mW[50], *i.e.* negligible when compared to the Fermi level shifts measured around 200 meV/mW. Furthermore, since the Seebeck coefficient is 0 for intrinsic graphene and since its sign changes with graphene doping type, the thermoelectric effect will tend to make the laser-exposed (hot) region evolve toward lower doping concentration. This is incompatible with our observations that the laser induces a doping type reversal for F1 (switching from p-type to n-type) and a n-type doping for F2, that was initially intrinsic. We thus tentatively attribute the observed effect to a local and reversible perturbation of the chemical equilibrium between graphene, the substrate and the atmosphere by laser-induced heating. The fast dynamics and the reversibility of the effect cannot be related to dopant removal but can be compatible with a temporary destabilization of O_2^- species. Noteworthy, graphene lying on SiO_2/Si exposed to H_2O alone, with only traces of O_2, has been shown to be n-doped[42]. Similarly, water significantly reduces hole doping of graphene deposited on mica[51]. The elucidation of the laser-assisted charge carrier density tuning mechanism deserves further investigations which are beyond the scope of this paper.

In conclusion, we have shown that a low power visible laser light can be used to reversibly tune the charge carrier density of graphene lying on a substrate, with subsecond characteristic time. This effect is highly sensitive to the substrate hydrophilicity and completely suppressed in suspended graphene. The continuous tuning of the doping in graphene from p-type to n-type has been achieved on O_2 plasma treated SiO_2/Si substrates. The observed phenomenon is attributed to a local and reversible perturbation of the chemical equilibrium established between graphene, the substrate and the atmosphere by laser-induced heating.

One technical implication of our study for the entire scientific community using Raman spectroscopy of graphene as a routine characterization technique is that it should be considered as potentially invasive as far as electronic properties are concerned. In particular, the laser induced-modification of graphene doping could account for recent discrepancies between Raman and electrical transport measurements[45]. It would be interesting to extend the present work to graphene on metals[47] and on silicon carbide[52] to assess how carefully Raman experiments on graphene must be performed.

On another hand, the ability to tune the charge carrier density with visible photons opens a wide set of opportunities to develop optically gated graphene electronic devices and a new approach to graphene optoelectronics. Finally, this effect should allow to study the interplay between graphene properties and the environment and to trigger laser-assisted functionalization of graphene leading to more advanced devices[53,54].

Methods

Sample fabrication. Four samples (F1 through F4) were prepared. They consisted of a 500 μm thick highly p-doped monocrystalline Si (100) substrate, with a thermal oxide layer of 290 ± 5 nm (in F1 and F3, oxide grown in O_2; in F2 and F4, oxide grown in H_2O) and a square matrix of metallic marks every 200 μm to ease the identification of graphene flakes. Samples F3 and F4 were further processed by etching matrices of 5 × 1 μm trenches with depths of 160 nm (F3) and 480 nm (F4) in between the metallic marks with a CF_4 ICP-RIE process.

Cleaning of F1 and F3 was performed by sonication in organic solvents (N-methyl-2-pyrrolidone, acetone and isopropanol; VLSI quality), immersion in piranha bath (H_2SO_4/H_2O_2 3 : 1) during 3 hours and Ar/O_2 (3 : 1) plasma cleaning in a Fischione 1020 for 20 min. On the other hand, F2 and F4 were cleaned by sonication in organic solvents and O_2 plasma cleaning in a PVA TePLA 300 at 800 W for 15 min. In addition, sample F2 was annealed during 1 hour at 400°C in a 300 sccm Ar flow at atmospheric pressure.

The contact angles of deionised water on three Si (100) substrates with a 290 ± 5 nm layer of thermal oxide (grown in H_2O atmosphere) have been measured by the sessile drop method. Sample CA1 was only rinsed in water and dried in a N_2 flux to eliminate silicon particles resulting from cleaving, sample CA2 was cleaned using the same procedure as for F1 and F3 (i.e. piranha plus light O_2 plasma), and sample CA3 was cleaned as F2 and F4 (i.e. strong O_2 plasma). The resulting advancing quasi-static contact angles were 60 ± 1° for CA1, unmeasurable or below 10° for CA2 and 18 ± 1° for CA3.

Finally, graphene was deposited on all samples by exfoliation from kish graphite with the scotch tape method[55].

Micro-Raman spectroscopy. Raman spectra were recorded using an Acton spectrometer fitted with a Pylon CCD detector and a 600 grooves/mm grating (~ 2.5 cm^{-1} between each CCD pixel). The samples were excited with a 532 nm (2.33 eV) CW frequency doubled Nd:Yag laser through a x100 objective (N.A. 0.9). The FWHM of the focused laser spot is 400 ± 20 nm. At 1 mW laser power, the power density impinging on the sample is thus about 800 kW cm^{-2} (8 mW μm^{-2}). Optimized focus conditions have been checked for each measurement. The samples are mounted on a three-axis piezoelectric stage to ensure the precise positioning and focusing of the laser spot. The maps were recorded with a 0.2 μm step in X (0.4 μm in Y) to probe the suspended graphene independently with a minimum of 2 to 3 points in the middle of the pool. The laser power was tuned with a variable neutral density filter controlled by a servomotor. The laser power was continuously measured by a calibrated photodiode put behind the beamsplitter. The whole experimental setup (spectrometer, piezoelectric stage, photodiodes, servomotor) were controlled by a dedicated and home-made Labview application. During laser power sweep or Raman mapping experiments, the acquisition times are varying from few seconds (2–5 s) at the highest power up to 30–60 s at the lowest power. The laser power sweep experiments typically last 20–60 min.

The results were reproduced on 8 hydrophilic samples (including F1 and F4, 3 others on 285 nm SiO_2/Si and 3 on 90 nm SiO_2/Si), 5 less hydrophilic substrates (including F2 and 4 on as-received SiO_2/Si substrates) and 3 suspended graphene flakes (including F3 and the suspended part of F4). All the flakes have been measured on different locations and the measurements have been repeated several times. On most of the samples Raman maps at different laser powers have also been measured.

1. Pisana, S. *et al.* Breakdown of the adiabatic Born-Oppenheimer approximation in graphene. *Nat Mater* **6**, 198–201 (2007).
2. Yan, J., Zhang, Y., Kim, P. & Pinczuk, A. Electric field effect tuning of electron-phonon coupling in graphene. *Phys. Rev. Lett.* **98**, 166802 (2007).
3. Das, A. *et al.* Monitoring dopants by Raman scattering in an electrochemically top-gated graphene transistor. *Nat Nanotechnol* **3**, 210–5 (2008).
4. Das, A. *et al.* Phonon renormalization in doped bilayer graphene. *Phys. Rev. B* **79**, 155417 (2009).
5. Chen, C.-F. *et al.* Controlling inelastic light scattering quantum pathways in graphene. *Nature* **471**, 617–620 (2011).
6. Mafra, D. L. *et al.* Using gate-modulated Raman scattering and electron-phonon interactions to probe single-layer graphene: a different approach to assign phonon combination modes. *Phys. Rev. B* **86**, 195434 (2012).
7. Kalbac, M. *et al.* The influence of strong electron and hole doping on the Raman intensity of chemical vapor-deposition graphene. *ACS Nano* **4**, 6055–6063 (2010).
8. Jung, N. *et al.* Charge transfer chemical doping of few layer graphenes: charge distribution and band gap formation. *Nano Letters* **9**, 4133–4137 (2009).
9. Zhan, D. *et al.* $FeCl_3$-based few-layer graphene intercalation compounds: single linear dispersion electronic band structure and strong charge transfer doping. *Advanced Functional Materials* **20**, 3504–3509 (2010).
10. Bruna, M. & Borini, S. Observation of Raman *G*-band splitting in top-doped few-layer graphene. *Phys. Rev. B* **81**, 125421 (2010).
11. Alzina, F. *et al.* Probing the electron-phonon coupling in ozone-doped graphene by Raman spectroscopy. *Phys. Rev. B* **82**, 075422 (2010).
12. Zhao, W., Tan, P., Zhang, J. & Liu, J. Charge transfer and optical phonon mixing in few-layer graphene chemically doped with sulfuric acid. *Phys. Rev. B* **82**, 245423 (2010).
13. Zhao, W., Tan, P. H., Liu, J. & Ferrari, A. C. Intercalation of few-layer graphite flakes with $FeCl_3$: Raman determination of Fermi level, layer by layer decoupling, and stability. *Journal of the American Chemical Society* **133**, 5941–5946 (2011).
14. Late, D. J. *et al.* Molecular charge-transfer interaction with single-layer graphene. *Journal of Experimental Nanoscience* **6**, 641–651 (2011).
15. Jung, N. *et al.* Optical reflectivity and Raman scattering in few-layer-thick graphene highly doped by K and Rb. *ACS Nano* **5**, 5708–5716 (2011).
16. Zhang, Z., Huang, H., Yang, X. & Zang, L. Tailoring electronic properties of graphene by π–π stacking with aromatic molecules. *The Journal of Physical Chemistry Letters* **2**, 2897–2905 (2011).
17. Medina, H., Lin, Y.-C., Obergfell, D. & Chiu, P.-W. Tuning of charge densities in graphene by molecule doping. *Advanced Functional Materials* **21**, 2687–2692 (2011).
18. Bruna, M. & Borini, S. Raman signature of electron-electron correlation in chemically doped few-layer graphene. *Phys. Rev. B* **83**, 241401 (2011).
19. Howard, C. A., Dean, M. P. M. & Withers, F. Phonons in potassium-doped graphene: the effects of electron-phonon interactions, dimensionality, and adatom ordering. *Phys. Rev. B* **84**, 241404 (2011).
20. Singh, A. K. *et al.* Molecular n-doping of chemical vapor deposition grown graphene. *J. Mater. Chem.* **22**, 15168–15174 (2012).
21. Crowther, A. C., Ghassaei, A., Jung, N. & Brus, L. E. Strong charge-transfer doping of 1 to 10 layer graphene by NO_2. *ACS Nano* **6**, 1865–1875 (2012).
22. Peimyoo, N., Yu, T., Shang, J., Cong, C. & Yang, H. Thickness-dependent azobenzene doping in mono- and few-layer graphene. *Carbon* **50**, 201–208 (2012).
23. Parret, R. *et al.* In situ Raman probing of graphene over a broad doping range upon Rubidium vapor exposure. *ACS Nano* **7**, 165–173 (2013).
24. Ferrari, A. C. *et al.* Raman spectrum of graphene and graphene layers. *Phys. Rev. Lett.* **97**, 187401 (2006).
25. Poncharal, P., Ayari, A., Michel, T. & Sauvajol, J.-L. Effect of rotational stacking faults on the Raman spectra of folded graphene. *Phys. Rev. B* **79**, 195417 (2009).
26. Lui, C. H. *et al.* Imaging stacking order in few-layer graphene. *Nano Letters* **11**, 164–169 (2011).
27. Havener, R. W., Zhuang, H., Brown, L., Hennig, R. G. & Park, J. Angle-resolved Raman imaging of interlayer rotations and interactions in twisted bilayer graphene. *Nano Letters* **12**, 3162–3167 (2012).
28. Kim, K. *et al.* Raman spectroscopy study of rotated double-layer graphene: misorientation-angle dependence of electronic structure. *Phys. Rev. Lett.* **108**, 246103 (2012).
29. Martins Ferreira, E. H. *et al.* Evolution of the Raman spectra from single-, few-, and many-layer graphene with increasing disorder. *Phys. Rev. B* **82**, 125429 (2010).
30. Venezuela, P., Lazzeri, M. & Mauri, F. Theory of double-resonant Raman spectra in graphene: intensity and line shape of defect-induced and two-phonon bands. *Phys. Rev. B* **84**, 035433 (2011).
31. Eckmann, A. *et al.* Probing the nature of defects in graphene by Raman spectroscopy. *Nano Letters* **12**, 3925–3930 (2012).
32. Mohiuddin, T. M. G. *et al.* Uniaxial strain in graphene by Raman spectroscopy: *G* peak splitting, Grüneisen parameters, and sample orientation. *Phys. Rev. B* **79**, 205433 (2009).
33. Lee, J. E., Ahn, G., Shim, J., Lee, Y. S. & Ryu, S. Optical separation of mechanical strain from charge doping in graphene. *Nat Commun* **3**, 1024 (2012).
34. Hulman, M., Haluška, M., Scalia, G., Obergfell, D. & Roth, S. Effects of charge impurities and laser energy on Raman spectra of graphene. *Nano Letters* **8**, 3594–3597 (2008).
35. Berciaud, S., Ryu, S., Brus, L. E. & Heinz, T. F. Probing the intrinsic properties of exfoliated graphene: Raman spectroscopy of free-standing monolayers. *Nano Letters* **9**, 346–352 (2009).
36. Ryu, S. *et al.* Atmospheric Oxygen binding and hole doping in deformed graphene on a SiO_2 substrate. *Nano Letters* **10**, 4944–4951 (2010).
37. Krauss, B. *et al.* Laser-induced disassembly of a graphene single crystal into a nanocrystalline network. *Phys. Rev. B* **79**, 165428 (2009).
38. Mitoma, N., Nouchi, R. & Tanigaki, K. Photo-oxidation of graphene in the presence of water. *The Journal of Physical Chemistry C* **117**, 1453–1456 (2013).
39. Zhang, W. & Li, L.-J. Observation of phonon anomaly at the armchair edge of single-layer graphene in air. *ACS Nano* **5**, 3347–3353 (2011).
40. Casiraghi, C. *et al.* Raman spectroscopy of graphene edges. *Nano Letters* **9**, 1433–1441 (2009).
41. Casiraghi, C. Doping dependence of the Raman peaks intensity of graphene close to the Dirac point. *Phys. Rev. B* **80**, 233407 (2009).
42. Levesque, P. L. *et al.* Probing charge transfer at surfaces using graphene transistors. *Nano Letters* **11**, 132–137 (2011).
43. Lafkioti, M. *et al.* Graphene on a hydrophobic substrate: doping reduction and hysteresis suppression under ambient conditions. *Nano Letters* **10**, 1149–1153 (2010).
44. Wang, R. *et al.* Control of carrier type and density in exfoliated graphene by interface engineering. *ACS Nano* **5**, 408–412 (2011).
45. Nagashio, K., Yamashita, T., Nishimura, T., Kita, K. & Toriumi, A. Electrical transport properties of graphene on SiO_2 with specific surface structures. *Journal of Applied Physics* **110**, 024513 (2011).
46. Lee, W. H. *et al.* Control of graphene field-effect transistors by interfacial hydrophobic self-assembled monolayers. *Advanced Materials* **23**, 3460–3464 (2011).
47. Shin, D.-W. *et al.* A facile route to recover intrinsic graphene over large scale. *ACS Nano* **6**, 7781–7788 (2012).
48. Xu, H., Chen, Y., Zhang, J. & Zhang, H. Investigating the mechanism of hysteresis effect in graphene electrical field device fabricated on SiO_2 substrates using Raman spectroscopy. *Small* **8**, 2833–2840 (2012).
49. Luo, Z., Pinto, N. J., Davila, Y. & Johnson, A. T. C. Controlled doping of graphene using ultraviolet irradiation. *Applied Physics Letters* **100**, 253108 (2012).
50. Zuev, Y. M., Chang, W. & Kim, P. Thermoelectric and magnetothermoelectric transport measurements of graphene. *Phys. Rev. Lett.* **102**, 096807 (2009).
51. Shim, J. *et al.* Water-gated charge doping of graphene induced by mica substrates. *Nano Letters* **12**, 648–654 (2012).
52. Sidorov, A. N. *et al.* Charge transfer equilibria in ambient-exposed epitaxial graphene on $(000\bar{1})$ 6H-SiC. *Journal of Applied Physics* **111**, 113706 (2012).
53. Wang, Q. H. *et al.* Understanding and controlling the substrate effect on graphene electron-transfer chemistry via reactivity imprint lithography. *Nat Chem* **4**, 724–732 (2012).

54. Georgakilas, V. *et al*. Functionalization of graphene: covalent and non-covalent approaches, derivatives and applications. *Chemical Reviews* **112**, 6156–6214 (2012).
55. Novoselov, K. *et al*. Electric field effect in atomically thin carbon films. *Science* **306**, 666–669 (2004).

Acknowledgments

This work was supported by the french ANR (Grafonics project ANR-10-NANO-0004) and has been done in the framework of the GDRI GNT 3217 "Graphene and Nanotubes: Science and Applications". MR-R acknowledges Beatriu de Pinós Marie Curie fellowship BP-0433 from AGAUR. A. Miranda is acknowledged for contributing to the design of substrates with trench arrays.

Author contributions

All authors (A.T., M.R.-R., M.P., J.-R.H., P.L., M.M., S.C., J.-L.S., E.D., A.-A.Z.) contributed extensively to the work presented in this paper.

Additional information

Supplementary information accompanies this paper at http://www.nature.com/scientificreports

Competing financial interests: The authors declare no competing financial interests.

How to cite this article: Tiberj, A. *et al*. Reversible optical doping of graphene. *Sci. Rep.* **3**, 2355; DOI:10.1038/srep02355 (2013).